Appl Nanosci (2016) 6:1119–1126
DOI 10.1007/s13204-016-0525-z

ORIGINAL ARTICLE

Visible-light photoactive Ag–AgBr/α-Ag_3VO_4 nanostructures prepared in a water-soluble ionic liquid for degradation of wastewater

Mohsen Padervand[1]

Received: 14 December 2015 / Accepted: 14 February 2016 / Published online: 2 March 2016

Abstract Ag–AgBr/α-Ag_3VO_4 photocatalysts, prepared by an ionic liquid-assisted precipitation method, were used as an efficient visible light-driven photocatalytic system for removal of wastewater and pathogenic bacteria from the aqueous medium. X-ray diffraction powder, diffuse reflectance spectroscopy, Fourier transform infrared, scanning electron microscopy, and nitrogen adsorption–desorption isotherm (BET) analysis methods were used to characterize the nanostructures. Photodegradation mechanism was investigated and the results showed that the prepared samples were too efficient for the degradation of Acid Blue 92 (AB92) azo dye, and *E. coli* cells under visible light. The photogenerated electron–hole pairs reacted with the species in the solution and produced super active radicals such as $OH^{\cdot}$, $HO^{\cdot}{}_2$, and $O^{\cdot -}{}_2$ which are responsible for the degradation of the environmental pollutions. TEM images were used to clarify the antibacterial activity of the products. Finally, as a practical application of the prepared photocatalysts, their ability evaluated for degradation of a real wastewater sample which was provided from the textile industries.

Keywords α-Ag_3VO_4 · Wastewater · Photodegradation · E. coli

✉ Mohsen Padervand
mohsenpadervand@gmail.com; padervand@maragheh.ac.ir

[1] Department of Chemistry, Faculty of Science, University of Maragheh, Maragheh, Tabriz, Iran

Introduction

Phtocatalytic treatment of water pollution using semiconductor-based materials has been considered as one of the most promising technologies to remove of toxic compounds from the environment. Over the past decades, the development of new visible-light photoactive materials has been pursued to improve the practical capacity of semiconductors under natural solar energy. To achieve this purpose, variant strategies such as doping the elemental impurities, coupling different semiconductors, and the synthesis of new visible-light photoactive catalysts have been served (Zhang et al. 2010; Lee et al. 2010; Yin et al. 2010; Kudo et al. 1998; Wang et al. 2008, 2010a, b; An et al. 2010).

Recently, due to their unique crystal structures and interesting photocatalytic properties, the ability of silver-based compounds such as Ag_3VO_4 (Konta et al. 2003; Hu and Hu 2007), Ag_2CO_3 (Dai et al. 2012), and Ag_3PO_4 (Yi et al. 2010; Bi et al. 2012) have been widely investigated for the degradation of organic pollutions under visible illumination. In spite of having suitable photoactivity, the high rate of electron–hole recombination makes the practical application of such materials limited. Moreover, corrosion of the semiconductor surface can take place during the photoreaction because of the conversion of Ag^+ ions to metallic Ag particles. To address this issue, recently, much effort has been focused on the development of new series of heterostructure materials, named plasmonic photocatalysts, which can lessen the mentioned limitations (Xiang et al. 2010; Chen et al. 2008). According to the reports the presence of metallic Ag and Au nanoparticles on the surface of Ag-based photocatalysts can improve their stability for repeated using (Kakuta et al. 1999; Wang et al. 2008, 2009). Inspired by these findings, many attempts have been performed to fabricate the highly efficient plasmonic

silver-based photocatalysts (Kuai et al. 2010; An et al. 2010; Xu et al. 2009).

In this paper we report our new attempts to prepare the visible light Ag–AgBr/α-Ag_3VO_4 photocatalysts by a facile precipitation method at the presence of a water-soluble ionic liquid which acted as a complexing agent and bromide source. Studying their photocatalytic activity for the degradation of AB92 and *E. coli* gram-negative bacteria revealed that the plasmonic nanostructures had higher activity than the pure α-Ag_3VO_4 sample. In addition, cycling experiments were performed to investigate the stability of as-prepared nanostructures after repeated using.

Experimental

Materials, instruments, and methods

$AgNO_3$ and NH_4VO_3 were used as silver and vanadium source, respectively. Tetra methyl ammonium hydroxide (TMAOH) was used as a template agent. During the synthesis procedure, 1-butyl-3-methylimidazolium bromide ([BMIM]Br) ionic liquid acted as the bromide source. All of the chemicals were purchased from Merck Co. and used without further purification. Double distilled water (DDW) was used during the preparation steps.

1.02 g of $AgNO_3$ was dissolved in 20 mL of DDW and the solution added drop by drop to a beaker contains 50 mL of water and 0.5 mL of TMAOH. The obtained yellow suspension was stirred vigorously while the color of precipitation changed to brown and then black. After 2 h of stirring at room temperature, a clear solution containing 0.233 g of NH_4VO_3 and [BMIM]Br (0.2 mL) in 30 mL of DDW was added slowly to the as-prepared suspension. This resulted in the formation of a yellow precipitation. The reaction medium was stirred for 0.5 h. The final product (Ag–AgBr/α-Ag_3VO_4) was filtered, washed repeatedly with DDW and methanol, and dried at 60 °C overnight. Preparation of pure α-Ag_3VO_4 was carried out in the same manner without adding any [BMIM]Br.

In all the experiments 0.02 g of photocatalysts was used and the used solvent was DDW. The visible illumination source was a 250-W OSRAM lamp. Total concentrations of the dye solution were easily determined using an UV spectrophotometer set at the λ_{max} of AB92 dye (574 nm).

Results and discussion

Characterization of the nanostructures

The formation process of the nanostructures can be described as follows:

$$(CH_3)_4N^+OH^-(H_2O) \rightarrow (CH_3)_4N^+(aq) + OH^-(aq) \quad (1)$$

$$Ag^+(aq) + 2OH^-(aq) \rightarrow Ag(OH)_2^-(aq) \quad (2)$$

$$2Ag(OH)_2^-(aq) \rightarrow Ag_2O_{(s)} + 2OH^-(aq) + H_2O \quad (3)$$

$$VO_4^{3-} + H_2O \rightarrow HVO_4^{2-} + OH^- \quad (4)$$

$$HVO_4^{2-} + 3Ag(OH)_2^- \rightarrow \alpha - Ag_3VO_4 + 5OH^- + H_2O \quad (5)$$

$$Ag_2O_{(s)} + 3(CH_3)_4N^+OH^- + Ag^+ + H_2O \rightarrow 2Ag(OH)_2^- + AgOH + 3(CH_3)_4N^+ \quad (6)$$

$$AgOH + OH^- \rightarrow Ag(OH)_2^- \quad (7)$$

Based on Eqs. 1–7, TMAOH facilitates the formation of $Ag(OH)_2^-$ intermediate which is a necessary step to complete the formation of the final products. In the next step, unstable $Ag(OH)_2^-$ species can convert to silver oxide and/or react with HVO_4^{-2} to form α-Ag_3VO_4. Besides, the solid Ag_2O particles react with TMAOH to prompt the formation of α-Ag_3VO_4.

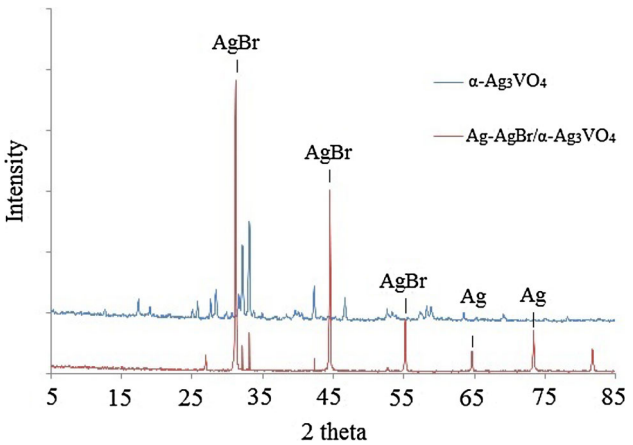

Fig. 1 The XRD patterns of prepared nanostructures

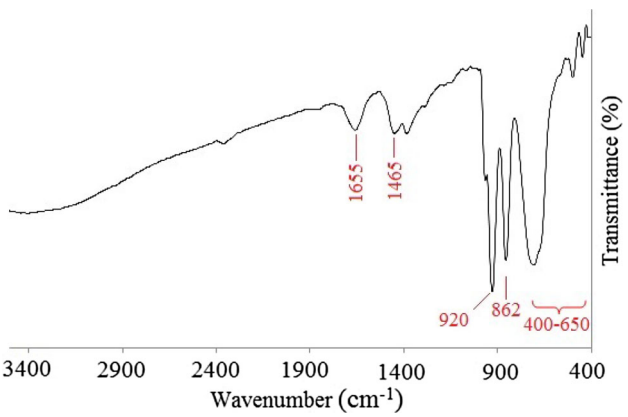

Fig. 2 The FTIR spectrum of prepared Ag–AgBr/α-Ag_3VO_4 sample

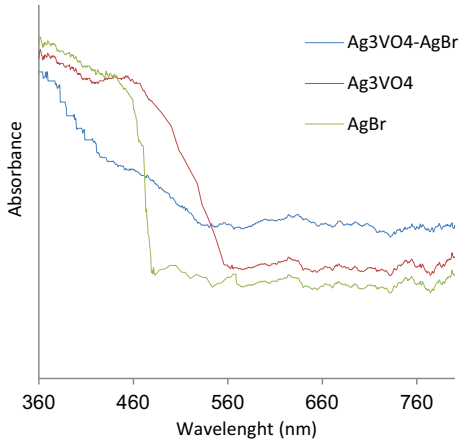

Fig. 3 The UV–vis spectra of the prepared photocatalysts

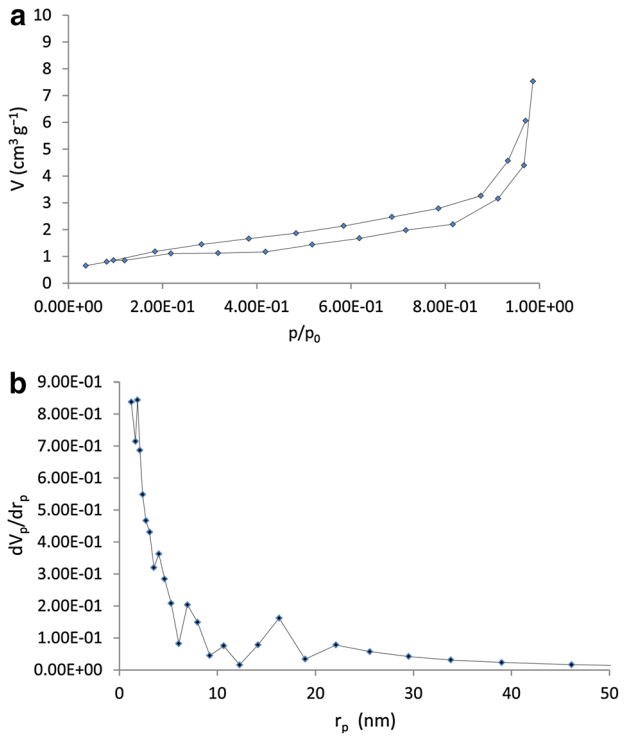

Fig. 4 A typical adsorption–desorption isotherm (**a**) and a BJH plot for Ag–AgBr/α-Ag_3VO_4 (**b**)

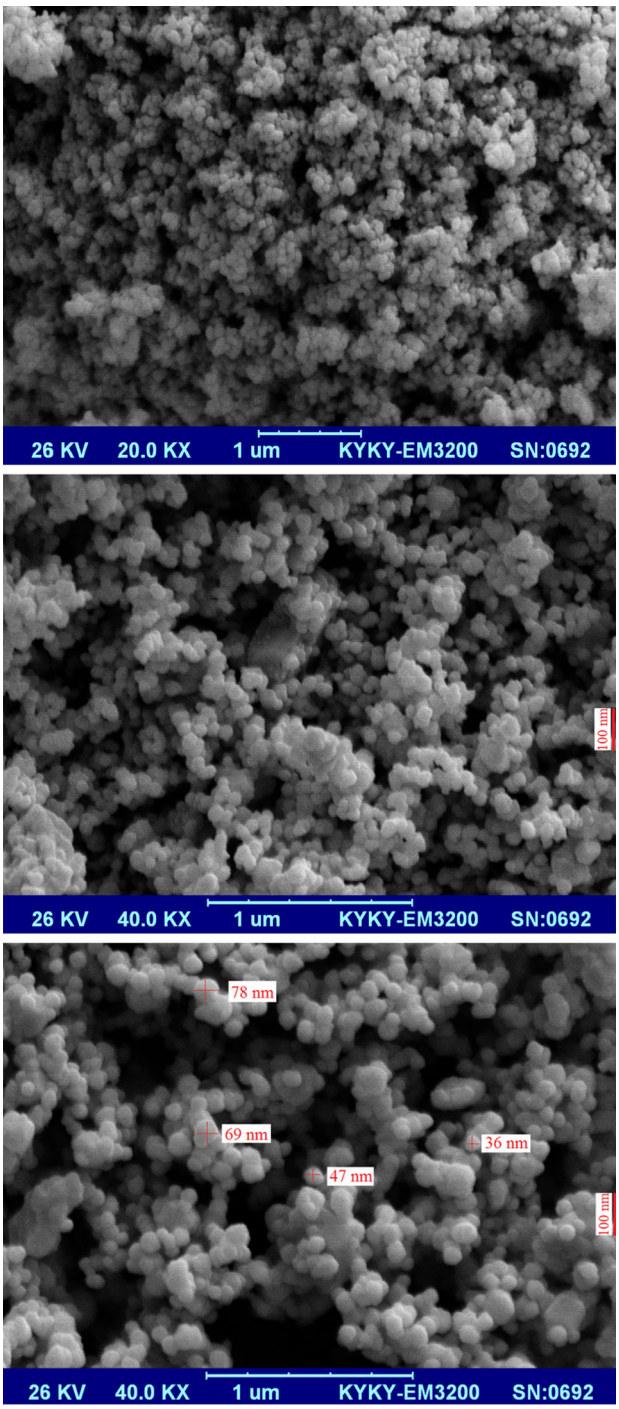

Fig. 5 Different magnification of SEM image of Ag–AgBr/α-Ag_3VO_4 sample

Because of the presence of [BMIM]Br ionic liquid in synthesis medium and the high reactivity of silver ions toward combination with the bromide anions, the following reactions could be occurred:

$$2Ag^{+} + NO_3^{-} + OH^{-} + [BMIM]^{+}Br^{-} \rightarrow Ag - OH - AgBr...[BMIM]^{+} + NO_3^{-} \quad (8)$$

$$Ag - OH - Ag - Br + OH^{-} \rightarrow Ag(OH)_2^{-} + AgBr \quad (9)$$

According to Eqs. 8 and 9, the formation of [BMIM] contained Ag–OH–Ag–Br species and its later reaction with the hydroxide ions promotes the formation of silver bromide phase of the photocatalysts.

The XRD patterns were used to investigate the phase structure of the samples and the results are shown in Fig. 1. All the sharp peaks at $2\theta = 32.5°$, 33.06°, 33.7°, 26.6°, 27.2°, and 47° in the pattern of silver methavanadate are

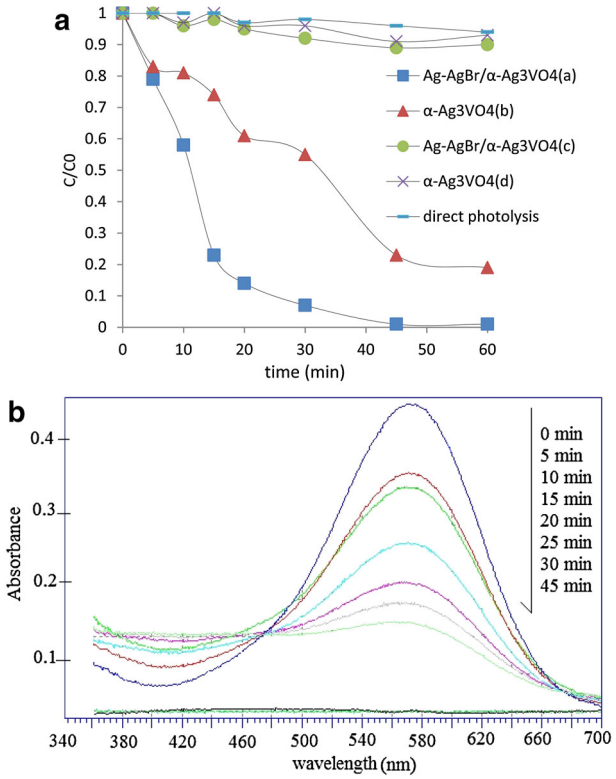

Fig. 6 **a** The results for the photodegradation of AB92 under illumination (**a**, **b**) and dark (**c**, **d**). **b** UV–vis spectrum of AB92 solution during the photocatalytic experiment (dye concentration: 20 ppm, catalyst dosage: 0.02 g, temperature: 27 °C)

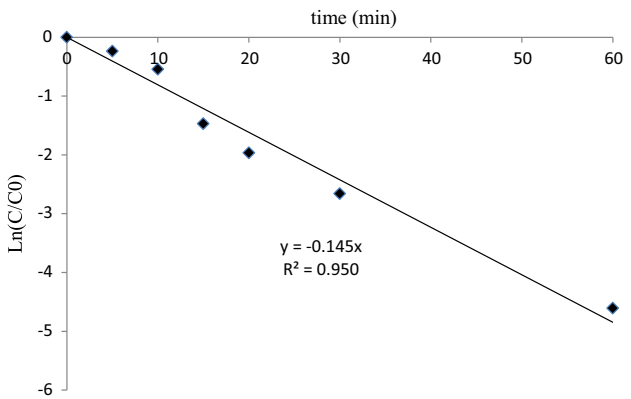

Fig. 7 Pseudo-first order kinetic of AB92 photodegradation over Ag–AgBr/α-Ag_3VO_4

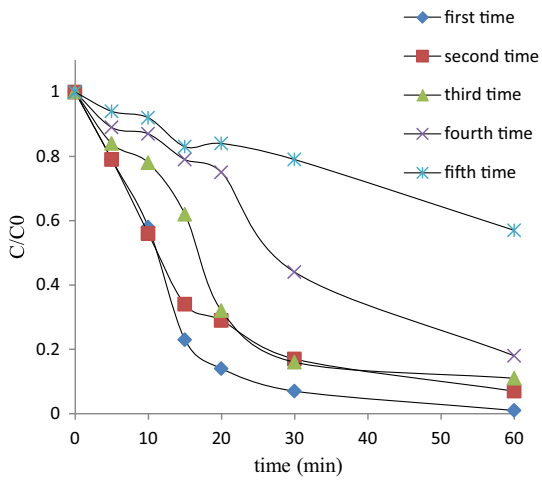

Fig. 8 The results of reuse-ability tests over Ag–AgBr/α-Ag_3VO_4 sample

indexed to the crystalline phase of α-Ag_3VO_4 ((JCPDS 43-054)). In addition, the peaks at 32.5°, 44.9°, and 55.1° are assigned to the silver bromide crystal phase structure which has a significant intensity compared to the characteristic peaks of α-Ag_3VO_4. Two observable peaks at 64.9° and 74° in the XRD pattern of Ag–AgBr/α-Ag_3VO_4 are the characteristic peaks of Ag° crystalline phase. However, we did not observe any characteristic peaks assigned to the silver nanocrystals in the pattern of α-Ag_3VO_4.

The FTIR spectrum of the final product (Ag–AgBr/α-Ag_3VO_4) recorded at 400–3500 cm^{-1} is shown in Fig. 2. The strong absorption bands at 400–650 cm^{-1} and the sharp one at 862 cm^{-1} are assigned to the symmetric and asymmetric vibrations of V–O–V bonds in the structures. Furthermore, the band at 920 cm^{-1} is the characteristic band of the bending vibrations of the terminal VO_4^{-3} groups (Chao-Ming et al. 2009). Peaks at wavenumbers of 1465 and 1655 cm^{-1} are assigned to the C=C and C=N stretching vibrations in the imidazolium ring of [BMIM]Br.

In order to determine the optical response of the prepared samples, we studied the UV–vis absorption spectra. From Fig. 3, the absorption onset is around 582 and 498 nm for α-Ag_3VO_4 and AgBr, respectively. This absorption extends into the higher wavelength (nearly 690 nm) for the Ag–AgBr/α-Ag_3VO_4 heteojunction photocatalyst. This observation is in agreement with the obtained results for the better photocatalytic activity of Ag–AgBr/α-Ag_3VO_4 under visible irradiation.

BET analysis was carried out to explain the porosity of the prepared samples and the results exhibited that the specific surface area is 31.00 and 19.84 $m^2\ g^{-1}$ for Ag–AgBr/α-Ag_3VO_4 and α-Ag_3VO_4 pure sample, respectively. Moreover, the results for the BJH analysis showed that the maximum distribution of the pore size in the final product is around 1.85 nm. Typical nitrogen adsorption–desorption isotherm and BJH curve of the final product is shown in Fig. 4a, b, respectively.

The surface morphology and microstructure of the samples have been examined by SEM. From Fig. 5, the uniform spherical nanostructures exhibit the regular morphology and the average size of the particles on the surface is around 57 nm. C.

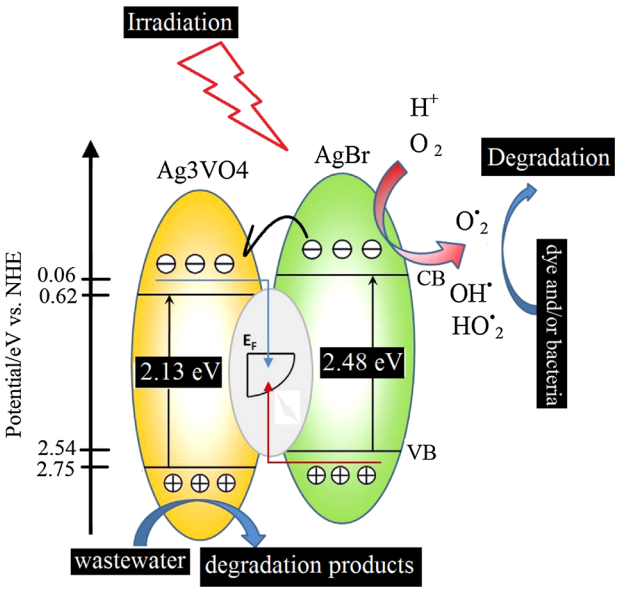

Scheme 1 Photodegradation of the wastewater over the prepared nanostructures

Photocatalytic removal of the bacteria and organic pollutants

The obtained results for the photodegradation of AB92 solution over the α-Ag_3VO_4-based nanostructures under visible illumination are shown in Fig. 6a, b. Comparing the rate and efficiency for bleaching of the dye solutions, we found that Ag–AgBr/α-Ag_3VO_4 plasmonic photocatalyst has better activity than the pure α-Ag_3VO_4 sample. As shown in Fig. 6a, the former case was able to completely destroy the chromophoric structure of AB92 in 15 min. As shown in Fig. 6b, which represents the UV spectrum of the dye solution illuminated in the presence of Ag–AgBr/α-Ag_3VO_4, the absorption in λ_{max} decreased dramatically by the treatment time.

According to the reports, a simplified Langmuir–Hinshelwood model could well describe the photoreaction kinetics of dye decomposition (Konta et al. 2003; Hu and Hu 2007; Dai et al. 2012; Yi et al. 2010; Bi et al. 2012). Based on this model, depicting $Ln(C/C_0)$ versus time gives a linear curve (Fig. 7) having the slope of 0.145 s^{-1}, where k is the pseudo-first-order rate constant. C_0 and C stand for the initial concentration and the concentrations after a certain reaction time, respectively.

To study the stability of the prepared nanostructures as a very important issue in the photocatalysis, we carried out the cycling tests by evaluating the decreased concentration of AB92 after repeated reactions while all the parameters were kept constant during the experiments. From Fig. 8, the rate and efficiency were smoothly decreased after four times of repeated using when we used Ag–AgBr/α-Ag_3VO_4 as photocatalyst and the activity just changed afterward. As a whole, the results demonstrate that the plasmonic Ag–AgBr/α-Ag_3VO_4 sample is a very stable visible light photocatalyst and it is promising for the industrial applications.

From the equation $E_g = 1239.8/\lambda$ (Anandan et al. 2009), the band gap energies were calculated to be 2.13 and 2.48 eV for α-Ag_3VO_4 and AgBr, respectively. To estimate the band structure of α-Ag_3VO_4 and AgBr we used the empirical formulas $E_{VB} = \chi - E_{e+}\ 0.5E_g$ and $E_{CB} = E_{VB} - E_g$, where E_{VB} and E_{CB} are the edge potential of valance and conduction bands (Katsumata et al. 2014; Bi et al. 2011). χ is the semiconductor electronegativity which is defined as the geometric mean of the electronegativity of the constituent atoms. Electronegativity of each atom is also defined as the arithmetic mean of its electron affinity and first ionization energy. The amount of χ was 6.19 and 5.8 eV for Ag_3VO_4 and AgBr, respectively. E_e (the energy of free electrons on the hydrogen scales) is about 4.5 eV versus NHE. As a result, E_{VB} and the corresponding E_{CB} were calculated to be 2.75 and 0.62 eV for Ag_3VO_4, and 2.54 and 0.06 eV for AgBr, respectively. From the UV–vis spectrum of Ag–AgBr/α-Ag_3VO_4, the absorption edge shifted to the higher wavelengths or lower energy which is in agreement with its better photoactivity. From Scheme 1, under irradiation, the electron–hole pairs are photogenerated on the surface of the photocatalyst. Because of the band gap energies (2.13 and 2.48 eV) both α-Ag_3VO_4 and AgBr can be photoexcited. The electrons can migrate to the conduction band of α-Ag_3VO_4 due to the more negative potential of AgBr conduction band (Qing et al. 2013). This process reduces the electron–hole recombination and enhances the photoactivity.

In order to prove the high photocatalytic capacity of Ag–AgBr/α-Ag_3VO_4, a real wastewater sample was obtained from the textile industry, diluted with DDW, and treated under the same conditions for the degradation experiment. As shown in Fig. 9, the absorption in all the wavelengths decreased dramatically which confirmed the

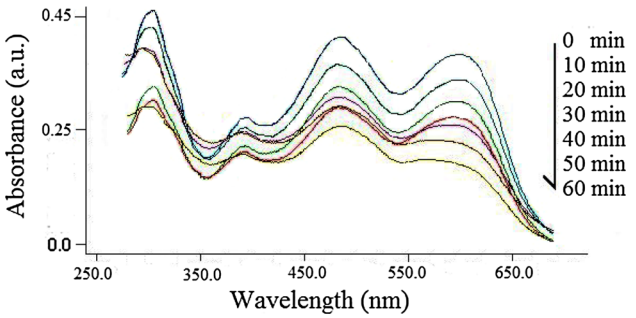

Fig. 9 The UV–vis spectrum for the photodegradation of a real wastewater under the same conditions over Ag–AgBr/α-Ag_3VO_4

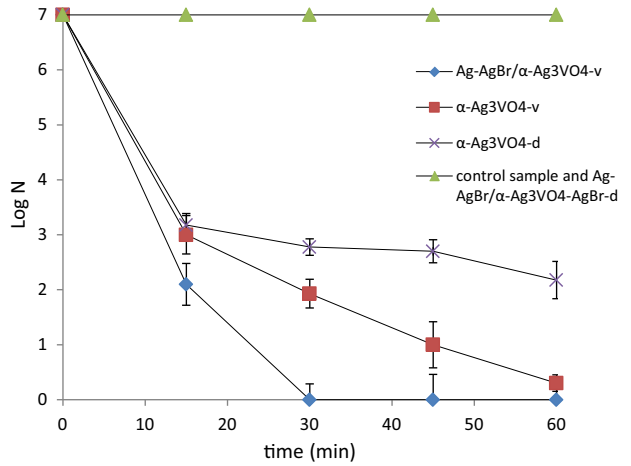

Fig. 10 The results of the antibacterial tests over the prepared photocatalysts

incredible photocatalytic properties of Ag–AgBr/α-Ag_3VO_4 nanostructure.

The obtained results for the antibacterial experiments over the prepared samples indicated that the nanostructures had high bactericidal effect on *E. coli* in water under visible irradiation. The results of the light control experiment indicate that no photolysis of the bacterial cells occurred under visible light. According to Fig. 10, the number of colonies formed in the cultivation medium decreased impressively up to 30 and 60 min when we used Ag–AgBr/α-Ag_3VO_4 and α-Ag_3VO_4 as photocatalyst, respectively. Super-active species included $OH^{\cdot}$, $HO^{\cdot}_2$, and HO_2^- radicals produced on the surface of nanostructures during the irradiation which can attack the microorganisms and destroy the cell walls. This well shows that the prepared nanostructures can be applied for the removal of pathogenic microorganisms from the wastewater under sun light. Furthermore, under dark conditions, the number of surviving bacteria was almost similar to that of observed for the control sample. This demonstrates that Ag–AgBr/Ag_3VO_4 has no toxic effect on *E. coli* cells. However, α-Ag_3VO_4 showed a significant antibacterial activity in the absence of visible light which may arise from the release of free silver ions bonded to the structure into the medium. To support this matter, we analyzed a filtered suspension treated by α-Ag_3VO_4 sample in the absence of irradiation source by Atomic Absorption Spectroscopy (Younglin, AAS8200 Model) to determine the silver content. However, the result of this analysis implied that there was not any free Ag in the solution. To explain the antibacterial mechanism of α-Ag_3VO_4 under dark, TEM analysis was performed on the damaged cell walls during the treatment time. Based on the TEM micrographs (Fig. 11), aggregation of the nanostructures around the outer membrane of the cell wall is the most probable mechanism for the

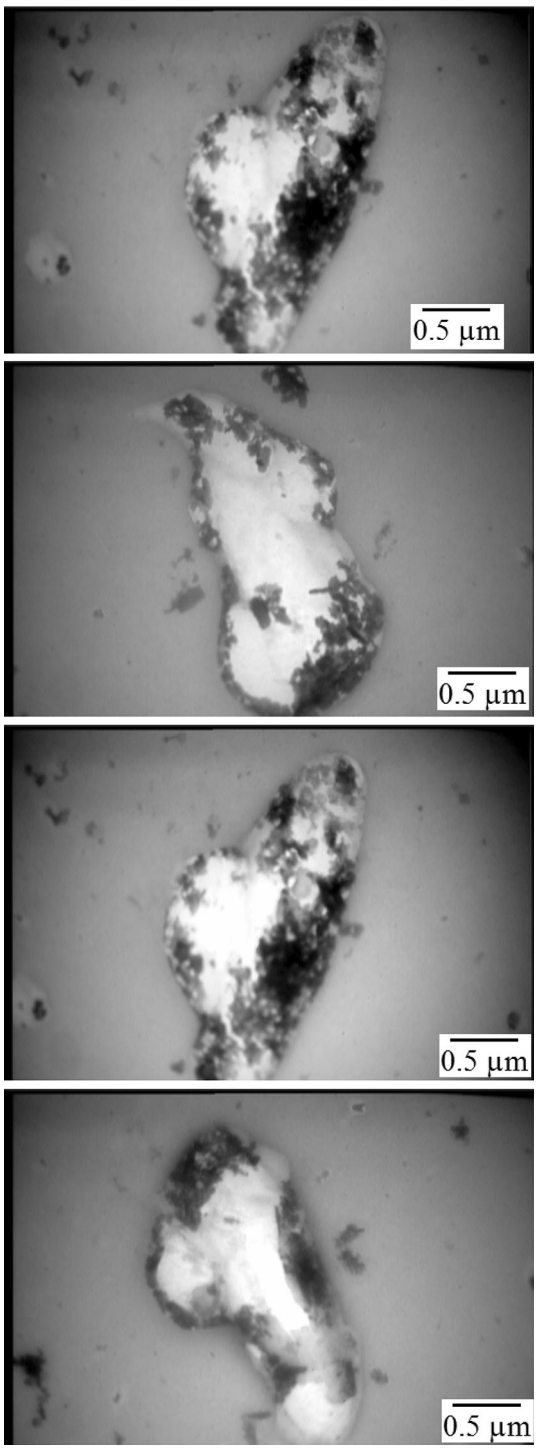

Fig. 11 TEM images of E.coli cell wall after the treatment time with α-Ag_3VO_4

bacteria inactivation. We suggest that bonding the VO_4^{-3} groups of the nanostructures to the lipopolysaccharides constituents of the bacterial cell wall blocked some vital channels where the microorganism nourishes via them. Lipopolysaccharides are located in the outer membrane of the cell wall and predominantly contain a specific lipid,

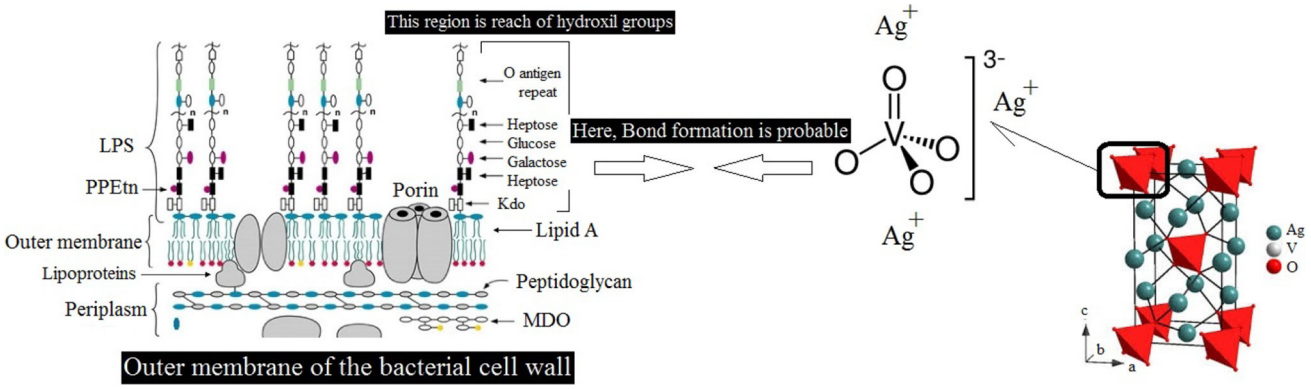

Scheme 2 The antibacterial mechanism over α-Ag_3VO_4 under dark conditions

named lipid A which contains many types of polar groups such as phosphate, hydroxyl, amino, and carboxylic. All of these functional segments are capable of making strong bonds with the vanadate groups of the nanostructures. This process is schematically shown in Scheme 2.

Conclusions

Plasmonic Ag–AgBr/α-Ag_3VO_4 nanostructures were prepared by an ionic liquid-assisted precipitation method. XRD, DRS, SEM, BET, and FTIR analysis methods well confirmed the formation of crystalline phase of the structures. From the UV–vis spectra, the absorption onset of pure α-Ag_3VO_4 was significantly changed in the presence of AgBr and its band gap shifted to the higher wavelength. The results for the photocatalytic degradation of AB92 and E.-coli bacterium revealed that the prepared nanostructures had incredible activity for the removal of wastewater under visible irradiation. In addition, according to the results of cycling experiments, the photocatalysts were stable under illumination which makes them suitable for the practical applications. To guarantee the photoactivity of the prepared catalysts toward decomposition of the real wastewaters under sun light, photodegradation of a wastewater sample produced by the textile industries was investigated and we found that the absorption in all wavelengths decreased significantly during the photocatalytic treatment. To explain the antibacterial mechanism of pure α-Ag_3VO_4 sample, TEM analysis was performed and the results showed that the most important reason for the antibacterial activity at dark is the aggregation of solid particles around the outer membrane of the cell wall which disturbs the microorganism nourishment.

References

An C, Peng S, Sun Y (2010) Facile synthesis of sunlight-driven AgCl: Ag plasmonic nanophotocatalyst. Adv Mater 22:2570–2574

Anandan S, Kathiravan K, Murugesan V, Ikuma Y (2009) Anionic (IO_3^-) non-metal doped TiO_2 nanoparticles for the photocatalytic degradation of hazardous pollutant in water. Catal Commun 10:1014–1019

Bi YP, Ouyang SX, Cao JY, Ye JH (2011) Facile synthesis of rhombic dodecahedral AgX/Ag_3PO_4 (X=Cl, Br, I) heterocrystals with enhanced photocatalytic properties and stabilities. Phys Chem Chem Phys 13:10071–10075

Bi YP, Hu HY, Ouyang SX, Lu GX, Cao JY, Ye JH (2012) Photocatalytic and photoelectric properties of cubic Ag_3PO_4 submicrocrystals with sharp corners and edges. Chem Commun 48:3748–3750

Chao-Ming H, Guan-Ting P, Yu-Chu ML, Min-Hsing L, Thomas CKY (2009) Crystalline phases and photocatalytic activities of hydrothermal synthesis Ag_3VO_4 and $Ag_4V_2O_7$ under visible light irradiation. Appl Catal A General 358:164–172

Chen X, Zhu HY, Zhao JC, Zheng ZF, Gao XP (2008) Visible-light-driven oxidation of organic contaminants in air with gold nanoparticle catalysts on oxide supports. Angew Chem Int Ed 47:5353–5356

Dai GP, Yu JG, Liu G (2012) A new approach for photocorrosion inhibition of Ag_2CO_3 photocatalyst with highly visible-light-responsive reactivity. J Phys Chem C 116:15519–15524

Hu XX, Hu C (2007) Preparation and visible-light photocatalytic activity of Ag_3VO_4 powders. J Solid State Chem 180:725–732

Kakuta N, Goto N, Ohkita H, Mizushima T (1999) Silver bromide as a photocatalyst for hydrogen generation from CH_3OH/H_2O solution. J Phys Chem B 103:5917–5919

Katsumata H, Hayashi T, Taniguchi M, Suzuki T, Kaneco S (2014) Highly efficient visible-light driven AgBr/Ag_3PO_4 hybrid photocatalysts with enhanced photocatalytic activity. Mater Sci Semicond Process 25:68–75

Konta R, Kato H, Kobayashi H, Kudo A (2003) Photophysical properties and photocatalytic activities under visible light irradiation of silver vanadates. Phys Chem Chem Phys 5:3061–3065

Kuai L, Geng BY, Chen XT, Zhao YY, Luo YC (2010) Facile subsequently light-induced route to highly efficient and

stable sunlight-driven Ag–AgBr plasmonic photocatalyst. Langmuir 26:18723–18727

Kudo A, Ueda K, Kato H, Mikami I (1998) Photocatalytic O_2 evolution under visible light irradiation on $BiVO_4$ in aqueous $AgNO_3$ solution. Catal Lett 53:229–230

Lee DK, Cho IS, Lee SW, Bae ST, Noh JH, Kim DW, Hong KS (2010) Effects of carbon content on the photocatalytic activity of $C/BiVO_4$ composites under visible light irradiation. Mater Chem Phys 119:106–111

Qing Z, Wan-Sheng W, Ling L, Gui-Qi G, Hong-Li G, Hong D, An-Wu X (2013) Facile synthesis of the novel Ag_3VO_4/AgBr/Ag plasmonic photocatalyst with enhanced photocatalytic activity and stability. J Phys Chem C 117:5894–5900

Wang P, Huang B, Qin X, Zang X, Dai Y, Wei J, Wangbo M (2008) Ag@AgCl: A highly efficient and stable photocatalyst active under visible light. Angew Chem Int Ed 47:7931–7933

Wang P, Huang BB, Zhang XY, Qin XY, Jin H, Dai Y, Wang ZY, Wei JY, Zhan J, Wang SY (2009) Highly efficient visible-light plasmonic photocatalyst Ag@AgBr. Chem Eur J 15:1821–1824

Wang JS, Li H, Li HY, Zou C (2010a) Mesoporous $TiO_{2-x}A_y$ (A=N, S) as a visible-light-response photocatalyst. Solid State Sci 12:490–497

Wang P, Huang B, Zang Q, Zang X, Qin X, Dai Y, Zang J, Yu J, Liu H, Lou Z (2010b) Highly efficient visible light plasmonic photocatalyst Ag@Ag(Br, I). Chem Eur J 16:10042–10047

Xiang Q, Yu J, Cheng B, Ong HC (2010) Microwave-hydrothermal preparation and visible-light photoactivity of plasmonic photocatalyst Ag-TiO_2 nanocomposite hollow spheres. Chem Asian J 5:1466–1474

Xu H, Li HM, Xu L, Wu CD, Sun GS, Xu YG, Chu JY (2009) Enhanced photocatalytic activity of Ag_3VO_4 loaded with rare-earth elements under visible-light irradiation. Ind Eng Chem Res 48:10771–10778

Yi ZG, Ye JH, Kikugawa N, Kako T, Ouyang SX, Stuart-Williams H, Yang H, Cao JY, Luo WJ, Li ZS (2010) An orthophosphate semiconductor with photooxidation properties under visible-light irradiation. Nat Mater 9:559–564

Yin WZ, Wang WZ, Sun SM (2010) Photocatalytic degradation of phenol over cage-like Bi_2MoO_6 hollow spheres under visible-light irradiation. Catal Commun 11:647–650

Zhang ZJ, Wang WZ, Shang M, Yin WZ (2010) Photocatalytic degradation of rhodamine B and phenol by solution combustion synthesized $BiVO_4$ photocatalyst. Catal Commun 11:982–986